LANGMUIR

pubs.acs.org/Langmuir Article

Unraveling Chiral Selection in the Self-assembly of Chiral Fullerene Macroions: Effects of Small Chiral Components Including Counterions, Co-ions, or Neutral Molecules

Jiancheng Luo, Songtao Ye, Putu Ustriyana, Benqian Wei, Jiahui Chen, Ehsan Raee, Yinghe Hu, Yuqing Yang, Yifan Zhou, Chrys Wesdemiotis, Nita Sahai, and Tianbo Liu*

Cite This: *Langmuir* 2020, 36, 4702−4710 Read Online

ACCESS | Metrics & More | Article Recommendations | Supporting Information

ABSTRACT: Lactic acid-functionalized chiral fullerene (C_{60}) molecules are used as models to understand chiral selection in macroionic solutions involving chiral macroions, chiral counterions, and/or chiral co-ions. With the addition of Zn^{2+} cations, the C_{60} macroions exhibit slow self-assembly behavior into hollow, spherical, blackberry-type structures, as confirmed by laser light scattering (LLS), transmission electron microscopy (TEM), and atomic force microscopy (AFM) techniques. Chiral counterions with high charge density show no selection to the chirality of AC_{60} macroions (LAC_{60} and DAC_{60}) during their self-assembly process, while obvious chiral discrimination between the assemblies of LAC_{60} and DAC_{60} is observed when chiral counterions with low charge density are present. Compared with chiral counterions, chiral co-ions show weaker effects on chiral selection with larger amounts needed to trigger the chiral discrimination between LAC_{60} and DAC_{60}. However, they can induce a higher degree of discrimination when abundant chiral co-ions are present in solution. Furthermore, the self-assembly of chiral AC_{60} macroions is fully suppressed by adding significant amounts of neutral molecules with opposite chirality. Thermodynamic parameters from isothermal titration calorimetry (ITC) reveal that chiral selection is controlled by the ion pairing and the destruction of solvent shells between ions, and meanwhile originates from the delicate balance between electrostatic interaction and molecular chirality.

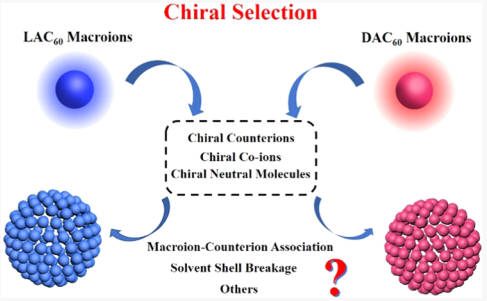

INTRODUCTION

Since Pasteur's discovery of molecular chirality,[1−3] homochiral self-sorting phenomena have been extensively documented in solid state, especially crystallization processes,[4−6] and later extended to the aggregation of amino acids in gas phase,[7−9] molecular interaction at the interface,[10,11] chemical reactions,[12−15] and supramolecular assemblies.[16−24] Despite the great efforts invested to understand the significance of homochirality in living systems (*e.g.*, L-amino acids and D-sugars during the evolution of life[25−27]), the origin of homochirality is still a matter of debate today.[28] How the tiny difference from molecular chirality is transmitted and amplificated, and consequently initiates recognition or selection phenomena during supramolecular self-assembly, is still an intriguing question. As the formation of supramolecular complexes is driven by noncovalent interactions, some studies attempted to explore chiral recognition or selection by using such interactions, including hydrogen bonding,[29−31] π interactions,[32,33] host−guest interaction,[34,35] electrostatic interaction,[36] *etc.* While these explorations mainly focus on different supramolecular structures achieved by chiral recognition/selection, a molecular-level understanding of chiral selection during supramolecular formation is still rare.

Biomacromolecules (*e.g.*, proteins) are often charged, *i.e.*, macroions.[37−39] In solution, three components are often essential for the behavior of macroions: counterions, co-ions, and neutral molecules such as solvents.[40−42] Since biomacromolecules possess complicate molecular structures and various conformations in response to the solution conditions,[43,44] some nanoscale molecules with a well-defined structure, size, and charge could be a valuable model to understand the origin of homochirality in nature. We previously reported that soluble ions with nanometer size (macroions), represented by polyoxometalates,[45] metal−organic nanocages,[46] and functional fullerenes (C_{60}),[47] can spontaneously self-assemble into single-layered, hollow, spherical supramolecular structures (blackberry-type) in solution. The kinetics of self-assembly process, as well as the final supramolecular structures, exhibits similarity to some bioprocesses such as virus capsid formation.[48] Moreover, the blackberry-type structures are highly sensitive to solution conditions[47,49−51] (*e.g.*, the type of counterions, co-ions, solvent polarity, and temperature),

Received: March 3, 2020
Revised: April 15, 2020
Published: April 15, 2020

https://dx.doi.org/10.1021/acs.langmuir.0c00611
Langmuir 2020, 36, 4702−4710

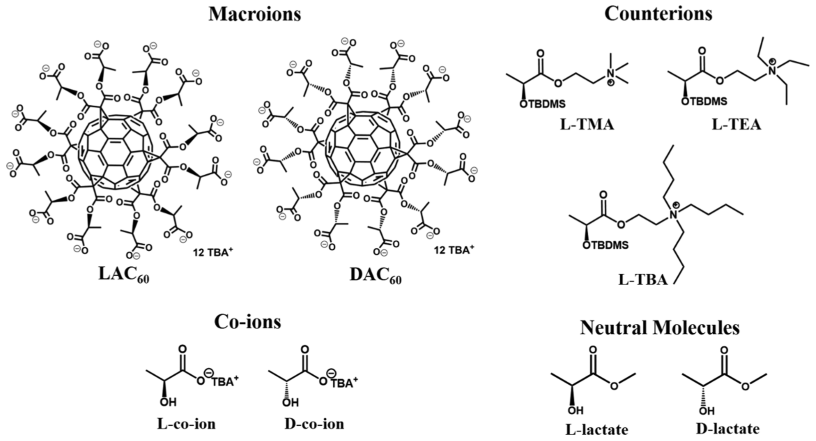

Figure 1. Molecular structures of chiral AC_{60} macroions, counterions, co-ions, and neutral molecules used in this study.

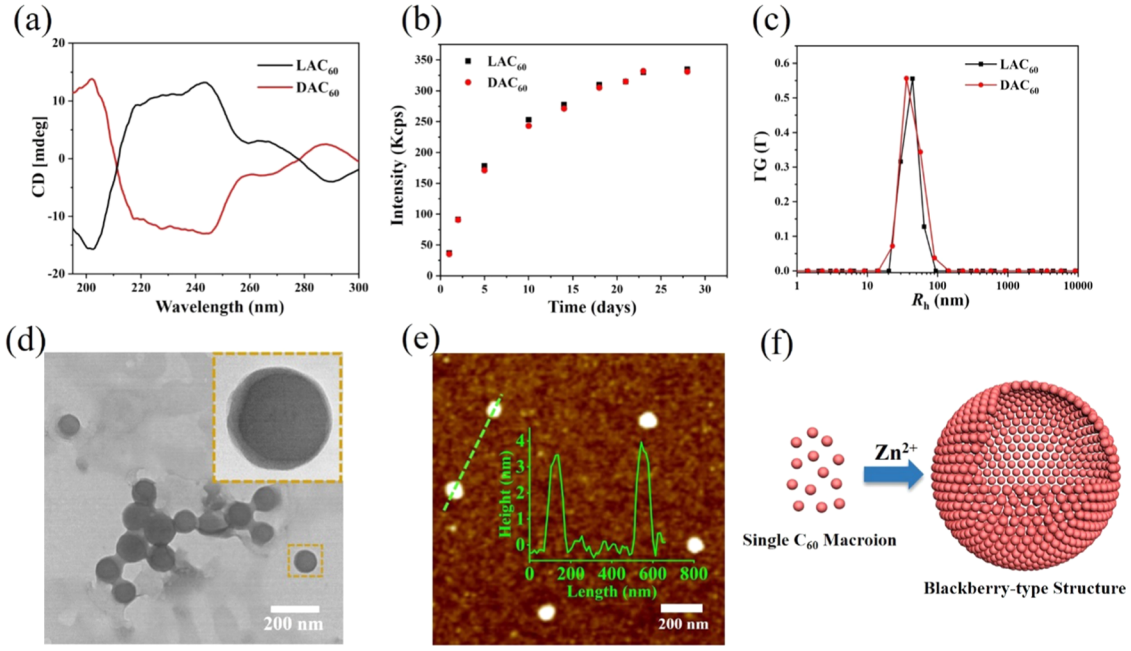

Figure 2. (a) CD spectra of LAC_{60} and DAC_{60} at the same solution concentration of 0.4 mg mL^{-1}. (b) Scattered intensities measured from 0.2 mg mL^{-1} LAC_{60} and DAC_{60} solutions with the addition of 10 equiv amounts of Zn^{2+} each. (c) CONTIN analysis of 0.2 mg mL^{-1} LAC_{60} and DAC_{60} solutions on the 23rd day. (d) TEM images of spherical assemblies. (e) AFM measurements of collapsed blackberries. (f) Schematic illustration of blackberry-type structures formed by chiral AC_{60} macroions.

making them good models to explore the interactions between macroions and other species in solution. Recently, we observed that two macroionic enantiomers tended to assemble into two types of chiral blackberries instead of mixed ones in their mixed solution, indicating an impressive chiral selection process that transmits the homochirality from molecular to supramolecular level.[36] The long-range electrostatic interaction is expected to play important roles behind this chiral recognition.

The next and more important question is how do these chiral macroions behave when they are in a chiral environment, *i.e.*, with other chiral components around them, such as chiral counterions, co-ions, or neutral molecules? Will these small chiral components have the same effect (identical interaction) on two macroionic enantiomers? If not, how significant can the difference be? We try to address these fundamental questions in this work, by using buckminsterfullerene (C_{60})[52−55] functionalized with chiral lactic acids (AC_{60}) on the surface. The anchored carboxylic acids make C_{60} fully hydrophilic, charged, and chiral. Two enantiomeric C_{60} macroions with identical chemical structure, size, and shape but opposite chirality (LAC_{60} and DAC_{60} in Figure 1) were synthesized, and they share similar features as macroions in polar solvents, as previously reported.[39] They are good models to explore interactions with small chiral species, including counterions, co-ions, and neutral molecules in solution, and consequently understand the effects of these small chiral components on chiral selection phenomena during supramolecular structure formation.

RESULTS AND DISCUSSION

Synthesis and Molecular Structure. The LAC_{60} and DAC_{60} macroions were prepared through the Bingel−Hirsch cyclopropanation reaction.[56−59] Each C_{60} was functionalized with 12 lactic acids and fully characterized by ^{1}H NMR, ^{13}C NMR, matrix-assisted laser desorption/ionization time-of-flight

https://dx.doi.org/10.1021/acs.langmuir.0c00611
Langmuir 2020, 36, 4702−4710

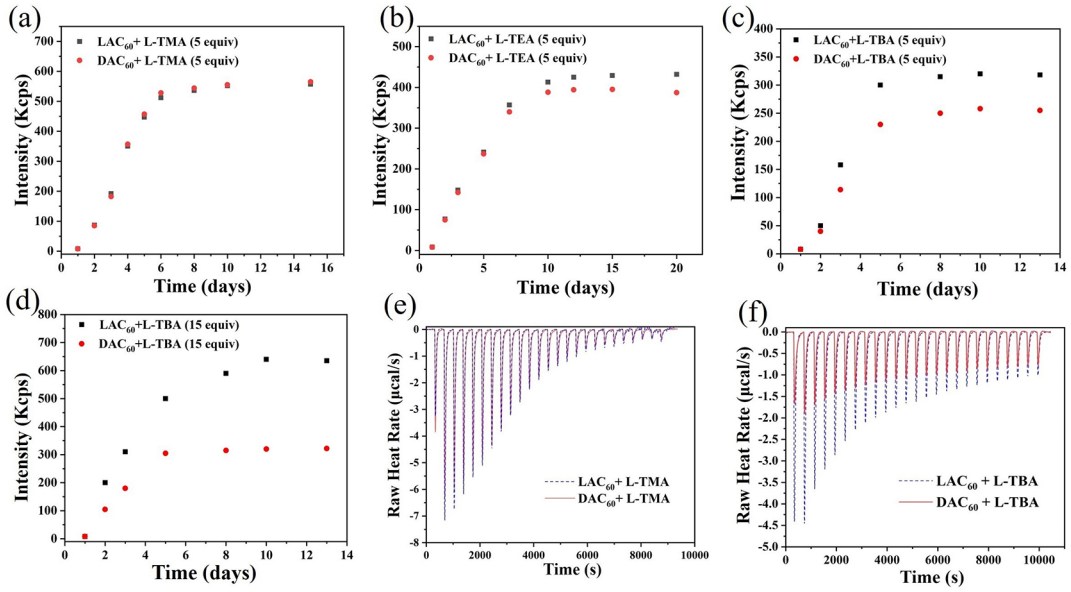

Figure 3. SLS measurements of LAC_{60} and DAC_{60} solutions when adding 5 equiv amounts of (a) L-TMA, (b) L-TEA, and (c) L-TBA, and (d) 15 equiv amounts of L-TBA. ITC titration curves of (e) L-TMA and (f) L-TBA into LAC_{60} and DAC_{60} solutions.

mass spectrometry (MALDI-TOF MS), and ultraviolet−visible (UV−vis) in Figures S1−S20. The chemical structures of chiral counterions, co-ions, and neutral molecules are shown in Figure 1 (detailed synthetic procedures and characterizations in Figures S21−S45).

Self-assembly of Chiral AC_{60} Macroions in Solution. The LAC_{60} and DAC_{60} have identical chemical composition, size, and charge number, with the only difference being chirality, as confirmed by circular dichroism (CD) measurements (Figure 2a). The AC_{60} with COOH groups (AC_{60}−COOH in Figure S19) has very limited solubility in water unless increasing the solution pH to 12. Therefore, acetonitrile is used for this study, in which the AC_{60} is quite soluble. Previously, we reported that the counterion-mediated attraction was an important driving force for the self-assembly of macroions.[60] To enhance the strength of the counterion-mediated attraction, the COOH groups are neutralized with tetrabutylammonium hydroxide (TBAOH; detailed procedure in the Supporting Information). In addition to the increase in charge density on the AC_{60} surface, extra divalent cations with strong binding with AC_{60} are added to enhance the macroion−counterion-mediated attraction. $ZnCl_2$ is chosen for this study due to its good solubility in acetonitrile. As monitored by static light scattering (SLS), the scattered intensities of 0.2 mg mL^{-1} LAC_{60} or DAC_{60} in MeCN slowly and continuously increase and become stable after a long time period (Figure 2b), indicating the formation of large supramolecular structures. The slow self-assembly kinetics of macroions, which usually takes several weeks or even months, has also been reported in our previous studies.[45,47] From the final scattered intensity, LAC_{60} and DAC_{60} solutions show no obvious difference. Moreover, the CONTIN analysis[61] of dynamic light scattering (DLS) measurements demonstrates that the hydrodynamic radii (R_h) of assemblies formed by LAC_{60} and DAC_{60} are identical (46 nm in Figure 2c), indicating that they have no difference when interacting with Zn^{2+}. The average radius of the spherical assemblies from transmission electron microscopy (TEM) measurements (51 ± 8 nm in Figure 2d) is consistent with that of DLS measurements. Furthermore, the radius of gyration (R_g) of the assemblies obtained from SLS measurements is 48 ± 3 nm (Figure S46), leading to the R_g/R_h ratio of 1.04, matching the theoretical value for a hollow sphere model (1.00).[62] Therefore, the hollow spheres have either a single layer or a few layers of AC_{60} molecules on their surface. The results from atomic force microscopy (AFM) measurements (Figure 2e) further confirm the single-layered model. The average height of the collapsed spheres after drying is 3.7 ± 0.3 nm (detailed analysis in Figures S47 and S48), which is close to two layers of AC_{60} macroions (diameter ∼1.5 nm), suggesting that the hollow spheres are likely to contain only one layer of AC_{60} on the surface. The combined results from light scattering, TEM, and AFM confirm that single-layered, hollow, spherical assemblies (blackberry-type structures) are formed in solution.

Effects of Counterions on the Chiral Selection of AC_{60} Macroions. The addition of Zn^{2+} cations leads to the formation of identical blackberry-type assemblies by LAC_{60} and DAC_{60}. The next question is the effects of chiral counterions. Figure 1 shows monovalent chiral counterions with increasing sizes from L-TMA to L-TEA and then to L-TBA, *i.e.*, decreasing charge density. For a typical experiment, two enantiomeric solutions (0.2 mg mL^{-1} LAC_{60} and DAC_{60}, each with 10 equiv of Zn^{2+}) were prepared, and additional chiral counterions (L-TMA, L-TEA, or L-TBA) were added into the solutions. For L-TMA (Figure 3a), LAC_{60} and DAC_{60} solutions have almost the same scattered intensity at equilibrium, indicating that L-TMA cannot induce chiral selection during the self-assembly of AC_{60} macroions. When larger counterions (L-TEA) are used, the final scattered intensity from the LAC_{60} solution is slightly higher than that from the DAC_{60} solution (Figure 3b). Moreover, the difference between LAC_{60} and DAC_{60} solutions is further magnified when even bulkier L-TBA counterions are applied (Figure 3c). DLS measurements show that the assembly sizes in LAC_{60} and DAC_{60} solutions are nearly identical with the presence of chiral counterions (Figures S49−S51), suggesting that the higher scattered intensity of LAC_{60} solutions is due to the higher number of assemblies in solution,[62] *i.e.*, LAC_{60} has a higher

https://dx.doi.org/10.1021/acs.langmuir.0c00611
Langmuir 2020, 36, 4702−4710

Table 1. Thermodynamic Parameters Fitted from ITC Titrations of Chiral Counterions into LAC_{60}/DAC_{60} Solutions

	n	ΔH (kJ mol^{-1})	$-T\Delta S$ (kJ mol^{-1})	ΔG (kJ mol^{-1})	K_a (M^{-1})
LAC_{60} + L-TMA	10.1 ± 0.5	−5.86 ± 0.24	−15.89 ± 0.37	−21.75 ± 0.12	(7.49 ± 0.36) × 10^3
DAC_{60} + L-TMA	10.8 ± 0.3	−3.83 ± 0.15	−17.79 ± 0.42	−21.62 ± 0.17	(7.12 ± 0.50) × 10^3
LAC_{60} + L-TBA	5.6 ± 0.8	−11.25 ± 0.48	−4.51 ± 0.13	−15.76 ± 0.21	(6.42 ± 0.54) × 10^2
DAC_{60} + L-TBA	4.7 ± 0.5	−3.44 ± 0.31	−10.45 ± 0.62	−13.89 ± 0.40	(2.98 ± 0.48) × 10^2

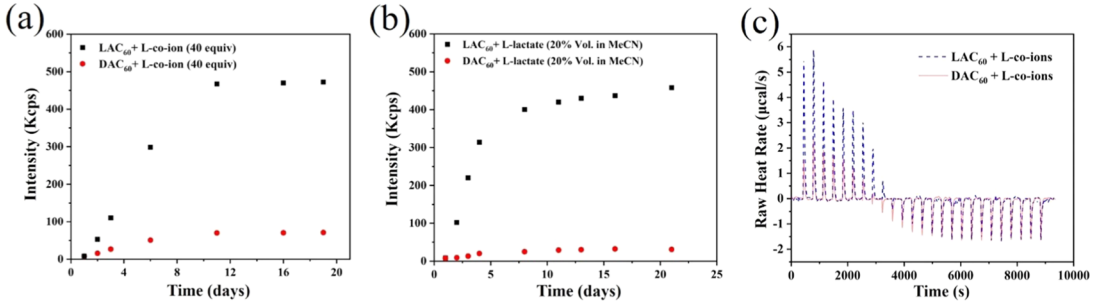

Figure 4. (a) SLS measurements of 0.2 mg mL^{-1} LAC_{60} and DAC_{60} solutions (MeCN, 10 equiv of Zn^{2+}) when adding 40 equiv of L-co-ions. (b) SLS measurements of 0.2 mg mL^{-1} LAC_{60} and DAC_{60} solutions (10 equiv of Zn^{2+}) with a solution condition of 20 vol % L-lactate in MeCN. (c) ITC titration curves of L-co-ions into LAC_{60} and DAC_{60} solutions.

tendency to form supramolecular structures with the help of L-counterions. Increasing L-TBA concentration further magnified the difference (Figure 3d).

It is intriguing that some chiral counterions can induce discrimination between the assemblies of two enantiomeric AC_{60}, while others cannot. To further understand this observation, isothermal titration calorimetry (ITC) is applied to determine the binding affinity (K_a) and other thermodynamic parameters such as enthalpy (ΔH) and entropy (ΔS) during the macroion−counterion interaction.[63,64] During the binding process, the macroion−counterion ion pairing leads to a thermodynamic change of $\Delta H < 0$ and $\Delta S < 0$, while the breakage of their solvent shells is a process with $\Delta H > 0$ and $\Delta S > 0$.[65−67] From ITC titration curves of L-counterions (L-TMA and L-TBA in Figure 3d,e, respectively), the macroion−counterion interaction shows exothermic peaks, suggesting that the ion pairing is dominant over the breakage of solvent shells due to the strong electrostatic interaction (macroion−counterion association). From Figure 3d, the heat releases between LAC_{60} + L-TMA and DAC_{60} + L-TMA titrations exhibit no significant difference, consistent with the SLS results that LAC_{60} and DAC_{60} assemble almost identically in the presence of L-TMA. The binding numbers (n) of two titrations (10.1 and 10.8 in Table 1) are close to the charge ratio of AC_{60}/L-TMA (12), indicating that L-TMA interacts strongly with chiral AC_{60} macroions and consequently can effectively replace the original counterions. In comparison, the titrations of L-TBA show that the heat release of LAC_{60} + L-TBA is higher than that of DAC_{60} + L-TBA, *i.e.*, stronger interaction between L-TBA and LAC_{60}. The binding numbers (n) from L-TBA titrations are less than those from L-TMA titrations due to the lower charge density of L-TBA (Table 1), which accordingly weakens their interactions with macroions and leads to partial replacement of the original counterions.

Interestingly, although the free energies ΔG of the two L-TMA titrations (LAC_{60} + L-TMA and DAC_{60} + L-TMA in Table 1) are very close, the contributions from entropy and enthalpy are quite different. Compared with DAC_{60}, the interaction between LAC_{60} and L-TMA has smaller ΔH to favor the lower ΔG. However, the interaction of LAC_{60} + L-TMA is entropically unfavored (larger ΔS). The enthalpy−entropy compensation leads to a similar level of ΔG between two L-TMA titrations. Therefore, L-TMA exhibits the same tendency to interact with two chiral AC_{60} macroions, regardless of their opposite chirality. When counterions with lower charge density are used (L-TBA), the enthalpy/entropy differences between LAC_{60} + L-TBA and DAC_{60} + L-TBA titrations are further magnified (Table 1). Moreover, the enthalpic advantage of LAC_{60} + L-TBA titration is dominant over its entropic disadvantage compared with DAC_{60} + L-TBA titration; consequently, the ΔG of LAC_{60} + L-TBA titration is lower than that of DAC_{60} + L-TBA titration, making the interaction between L-TBA and LAC_{60} more preferred—also matching our SLS observations that the final scattered intensity of LAC_{60} + L-TBA solution is higher than that of DAC_{60} + L-TBA (Figure 3c,d). For molecules with special shapes such as helices or macrocycles,[68−70] the entropic advantages, originated from a more condensed packing of one enantiomer over the other, are widely reported as an important reason for the chiral selection. However, the chiral AC_{60} is spherical. Meanwhile, the preferred interaction of LAC_{60} + L-TBA is largely due to enthalpy[66] (from macroion−counterion association; Figure 5a), as confirmed by the ITC, suggesting that the chiral selection here is quite different from the geometry-induced ones reported earlier. Therefore, the chiral AC_{60} is a good model to understand the chiral selection process controlled by the electrostatic interaction.

Effect of Co-ions on the Chiral Selection of AC_{60} Macroions. In solution, co-ions have the same type of charge as macroions. The electrostatic repulsion forces them away from the central macroions, and they are expected to have less impact on the solution behavior of macroions. A common effect of co-ions is to stabilize single macroions by forming an external layer outside the layer of associated counterions.[71−73] However, co-ion effects are ubiquitous in various systems such as chemistry and biology.[74−77] Our group also reported strong co-ion effects on the self-assembly of charged metal−organic macrocycles[78] and chiral polyoxometalates.[36] Therefore, it is interesting to explore co-ion effects on chiral selection.

https://dx.doi.org/10.1021/acs.langmuir.0c00611
Langmuir 2020, 36, 4702−4710

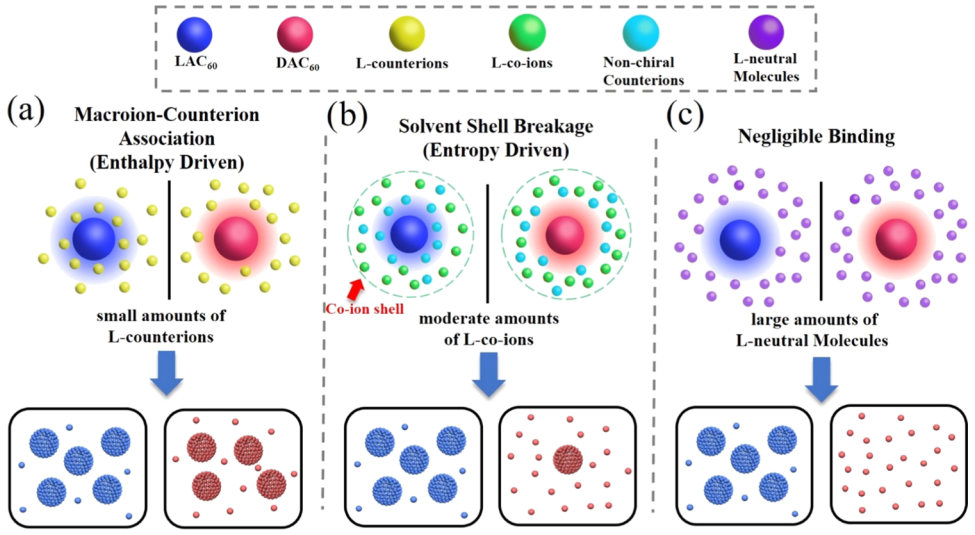

Figure 5. (a) Schematic illustration showing the effects of chiral counterions (a), chiral co-ions (b), and chiral neutral molecules (c) on the self-assembly and chiral selection during the blackberry formation of LAC_{60} and DAC_{60}. In counterion case (a), the preferred interaction between LAC_{60} and L-counterions attracts more counterions closely associated with LAC_{60} macroions. In the co-ion case (b), the stronger interaction between L-co-ions and DAC_{60}−counterion system leads to less solvent shell breakages of macroions by attracting more counterion away from the central macroions and therefore suppresses the self-assembly of DAC_{60}. While in the neutral molecule case (c), the binding between chiral C_{60} macroions and chiral neutral molecules is negligible. In each figure, the rest of counterions, co-ions, or neutral molecules are omitted for clarity.

Table 2. Thermodynamic Parameters Fitted from ITC Titrations of Chiral Co-ions into LAC_{60}/DAC_{60} Solutions

	n	ΔH (kJ mol^{-1})	$-T\Delta S$ (kJ mol^{-1})	ΔG (kJ mol^{-1})	K_a (M^{-1})
LAC_{60} + L-co-ion	9.1 ± 0.5	3.70 ± 0.30	−28.70 ± 0.71	−25.00 ± 0.45	(2.85 ± 0.52) × 10^4
DAC_{60} + L-co-ion	8.6 ± 0.6	1.99 ± 0.13	−25.42 ± 0.56	−23.43 ± 0.46	(1.49 ± 0.28) × 10^4

For counterions (L-TBA in Figure 3c), the obvious difference between LAC_{60} and DAC_{60} solutions can be observed when small amounts of L-TBA counterions (5 equiv) are added. In the case of co-ions, the amount needed to trigger a noticeable difference between LAC_{60} and DAC_{60} is larger (20 equiv, Figure S52), indicating that chiral co-ions have weaker effects. By adding 40 equiv of L-co-ions into LAC_{60} and DAC_{60} solutions, respectively, LAC_{60} solutions show faster self-assembly rate with higher scattered intensity at equilibrium, while the self-assembly of DAC_{60} is significantly suppressed (Figure 4a). When replacing L-co-ions with D-co-ions, the self-assembly of DAC_{60} is promoted and LAC_{60} solutions show lower scattered intensity (Figure S53). Surprisingly, although the effects of chiral co-ions are weaker than chiral counterions in terms of the concentration needed to initiate a noticeable difference between LAC_{60} and DAC_{60} solutions, chiral co-ions can induce a more significant difference when abundant co-ions are present. For example, the maximum difference in the amount of final assemblies (LAC_{60}/DAC_{60}) achieved by chiral counterions is 2.0 (15 equiv of L-TBA, Figure 3d), while the maximum difference (LAC_{60}/DAC_{60}) in the case of chiral co-ions is 6.6 when 40 equiv of L-co-ions is added (Figure 4a). With the further addition of chiral counterions or chiral co-ions, the blackberry-type structures start to become unstable due to the high ionic strength.[49] This result suggests that co-ions can induce stronger chiral selection than counterions. When the interactions between macroions and nearby molecules are too strong, it considerably eliminates the difference (D and L) originated from molecular chirality. Observations from the chiral counterion experiments also support this speculation. Among the three counterions (L-TMA, L-TEA, and L-TBA), L-TMA has the strongest electrostatic interaction with chiral AC_{60} macroions; as a result, LAC_{60} and DAC_{60} solutions show almost no difference in response to L-TMA.

ITC studies are further applied to understand the effect of co-ions by exploring how the presence of chiral co-ions impacts the macroion−counterion interaction during ITC titration. Unlike exothermic peaks observed from the titrations of different chiral counterions, the titrations of salts involving chiral co-ions show overall endothermic processes (Figure 4c), indicating that the breakage of solvent shells ($\Delta H > 0$) is dominant over the ion pairing ($\Delta H < 0$).[66] The co-ions are usually believed to stay outside the counterion layer, which is associated with a central macroion, and provide an additional shell to further stabilize the individual macroion (Figure 5b),[72,79] making the macroion−macroion attraction (and their self-assembly) more difficult. If the co-ions tend to interact with the counterion−macroion system stronger, their presence tends to attract the counterions slightly away from the macroions, leading to a less degree of solvent shell breakage of macroions. ITC titration curves show that the L-co-ions + LAC_{60} interaction can absorb more energy than the L-co-ions + DAC_{60} interaction (Figure 4c), suggesting less effective destruction of solvent shells in DAC_{60} solutions. Fitting the ITC data reveals that the enthalpy of DAC_{60} + L-co-ion titration is lower than that of LAC_{60} + L-co-ion titration (Table 2), which again confirms a less degree of solvent shell breakage of DAC_{60}. That is, the L-co-ions tend to interact with the counterion−DAC_{60} system stronger and consequently stabilize the single DAC_{60} more effectively. This is consistent with the SLS studies that the self-assembly in L-co-ions + DAC_{60} solution has been suppressed significantly compared with that in L-co-ions + LAC_{60} solution. Interestingly, although the

https://dx.doi.org/10.1021/acs.langmuir.0c00611
Langmuir 2020, 36, 4702−4710

interaction between LAC_{60} and L-co-ions is energetically unfavored (higher ΔH) compared with that of DAC_{60} + L-co-ions, the entropic gain of LAC_{60} + L-co-ion titration is much higher and eventually overcomes its disadvantage in enthalpy. As a result, the free energy ΔG of LAC_{60} + L-co-ion titration is lower than that of DAC_{60} + L-co-ion titration, making the interaction between L-co-ions and LAC_{60} preferred over DAC_{60}. Therefore, the chiral selection induced by chiral co-ions is controlled by the entropic gain (related to the solvent shell breakage, shown in Figure 5b), which is completely different from the chiral counterions that the chiral selection is mainly attributed to the difference in enthalpy (related to macroion−counterion association, shown in Figure 5a).

Effects of Neutral Molecules on the Chiral Selection of AC_{60} Macroions. Chiral methyl lactates (L-lactate and D-lactate in Figure 1) are used to explore whether chiral neutral molecules can impact the self-assembly of LAC_{60} and DAC_{60}. Without charge, their interactions with macroions are supposed to be negligible (Figure 5c). Indeed, ITC titrations of lactates into chiral AC_{60} solutions (Figure S54) show that the energy levels are close to background titrations (lactates into solvent), suggesting a very weak interaction between lactates and AC_{60}. From SLS measurements, LAC_{60} and DAC_{60} solutions show almost identical self-assembly rate even with the addition of 100 equiv of L-lactate (~0.3 vol % in MeCN; Figure S55), again confirming the very weak effect of lactates. Interestingly, when the added lactates (*e.g.*, L-lactate) further increase to extremely large amounts (5 vol % in MeCN, ~1600 equiv), LAC_{60} and DAC_{60} solutions start to exhibit different self-assembly rates, as well as scattered intensity at equilibrium (Figure S56). By further increasing the amounts of L-lactate to 20 vol % in MeCN, the difference becomes more significant, and the self-assembly of DAC_{60} is fully suppressed (Figure 4b). Unlike counterions and co-ions, which can bind to macroions within a certain length scale (electric double layer[80,81]), the neutral molecules are evenly distrusted in solution because they almost do not interact with macroions. Therefore, the amounts of neutral molecules to trigger chiral selection should be considerably higher than those of counterions/co-ions. However, with the absence of electrostatic interaction, the difference (D and L) from molecular chirality will play the major roles. Moreover, the macroions can stay stable with very large amounts of neutral molecules; eventually, in solution with concentrated chiral neutral molecules, the degree of chiral selection (14.9 in Figure 4b) is observed to be higher than the values from chiral counterions (2.0 in Figure 3c) and co-ions (6.6 in Figure 4a).

CONCLUSIONS

The self-assembly of two C_{60}-based chiral macroions into blackberry-type supramolecular structures is studied in the presence of chiral counterions, chiral co-ions, and chiral neutral molecules, respectively, aiming to understand their effects on inducing the chiral selection during the supramolecular structure formation. High-charge-density chiral counterions (L-TMA) do not show chiral selection feature, while low-charge-density chiral counterions (L-TBA) show obvious discrimination between LAC_{60} and DAC_{60} (favoring LAC_{60}). Chiral co-ions can also demonstrate the chiral selection phenomenon, but larger amounts are needed; however, they can induce a higher degree of selection than counterions. ITC measurements reveal that the chiral selection induced by counterions is mainly controlled by enthalpic advantages originating from the macroion−counterion ion pairing, while entropic advantages from the solvent shell breakage of macroions are responsible for the chiral selection in the case of co-ions. Chiral neutral molecules do not interact electrostatically with macroions; therefore, their impact on the chiral selection of macroions requires a very high concentration of chiral neutral molecules, and the macroions can stay stable under such condition. A very high degree of chiral selection can be achieved with the abundant chiral neutral molecule solution. This study unveils different reasons and impacts of chiral counterions, chiral co-ions, and chiral neutral molecules on the chiral selection in macroionic solutions. In the future, other chiral macroions, which are suitable for the studies in aqueous solution, will be explored.

EXPERIMENTAL SECTION

Dynamic Light Scattering (DLS) and Static Light Scattering (SLS). Both DLS and SLS measurements were performed on a Brookhaven Instruments light scattering spectrometer equipped with a diode-pumped solid-state (DPSS) laser operating at 532 nm and a BI-9000AT multichannel digital correlator. The SLS was performed over a broad range of scattered angles from 40 to 90°, with 2° interval. The radius of gyration (R_g) was calculated by using a partial Zimm plot derived from the Rayleigh−Gans−Debye equation. The partial Zimm plot was obtained from the following approximate formula: $1/I = C(1 + R_g^2 q^2/3)$. The R_g was determined from the slope and intercept of a plot of $1/I$ *vs* q^2. For DLS measurements, the intensity−intensity time correlation functions were analyzed by the constrained regularized (CONTIN) method. The average apparent translational diffusion coefficient, D_{app}, was determined from the normalized distribution function of the characteristic line width, $\Gamma(G)$. The hydrodynamic radius (R_h) was converted from D through the Stokes−Einstein equation: $R_h = KT/6\pi\eta D$, where K is the Boltzmann constant and η is the viscosity of the solvent at temperature T.

Nuclear Magnetic Resonance (NMR). Both ^{1}H NMR and ^{13}C NMR were measured on a Varian NMRS 500 spectrometer equipped with a 5 mm dual-broad-band probe. Noise reduction was performed when appropriate.

Transmission Electron Microscopy (TEM). TEM images were taken on a JEOL JEM-1230 electron microscope operated at 120 kV. Samples for TEM analysis were prepared by dropping a small volume of solution on the copper grid and drying under an oil pump; the average radius of assemblies was calculated based on the measured size of spheres in the TEM image.

Matrix-Assisted Laser Desorption/Ionization Time-of-Flight (MALDI-TOF) Mass Spectroscopy. MALDI-TOF mass spectra were measured on a Bruker Ultraflex III TOF/TOF mass spectrometer (Bruker Daltonics). Trans-2-[3-(4-*tert*-butylphenyl)-2-methyl-2-propenylidene] malononitrile (DCTB) was used as the matrix compound. The sample was prepared by depositing a 0.5 μL matrix solution on the wells of a 384-well ground-steel plate and depositing 0.5 μL of the sample solution on a spot of dried matrix and then adding another 0.5 μL matrix solution on top of the dried sample. Mass spectra were measured in the reflection mode, and the mass scale was calibrated externally with PS standards with similar molecular weights to those of the samples under consideration. Data analyses were conducted with Bruker's Flex Analysis software.

Isothermal Titration Calorimetry (ITC). The ITC measurements were conducted on a commercial TA Instruments Nano ITC system. The instrument was equipped with a 1.0 mL sample cell and an identical reference cell with an adiabatic shield in a vacuum-tight chamber. For a typical experiment, 1.0 mL LAC_{60} or DAC_{60} acetonitrile solutions were loaded into the sample cell, and the reference cell was filled with 1.0 mL acetonitrile. Chiral counterion, co-ion, or neutral molecule solutions (MeCN) were loaded into a 250 μL titration syringe and titrated into the sample cell with 10 μL as the interval. The background heat was subtracted by titrating the same concentration of counterion, co-ion, or neutral molecule solutions

https://dx.doi.org/10.1021/acs.langmuir.0c00611
Langmuir 2020, 36, 4702−4710

into acetonitrile. All thermodynamic parameters were fitted by the independence model. The error bars were calculated based on the fitting curves (with a 95% confidence level) by using NanoAnalyze software.

Circular Dichroism (CD). The CD measurements were performed on a Jasco J-1500 Series circular dichroism spectropolarimeter in a 1 mm cuvette (J/0556, Jasco). The range of measurement was set as 195−300 nm, and the LAC_{60} or DAC_{60} solution was prepared in acetonitrile at a concentration of 0.4 mg mL^{-1}. Each measurement was conducted at 25 °C using a data pitch of 0.2 nm, a 2 nm bandwidth, a response time of 4 s, and a scan speed of 50 nm min^{-1}. Six accumulations were averaged for each measurement.

Ultraviolet−Visible Spectroscopy (UV−Vis). UV−vis experiments were performed on an Agilent Technologies 8453 UV−vis spectrophotometer and analyzed by UV−vis ChemStation Software.

Atomic Force Microscope (AFM). AFM measurements were performed on a Dimension Icon AFM (Bruker AXS). Samples were prepared by drop-casting the solution onto silica substrates. Tapping mode and a Bruker AFM tip (RTESPA-150) were used.

Sample Preparation. The preparation of LAC_{60} and DAC_{60} can be found in the Supporting Information. Since the AC_{60} can only be dissolved in high pH water (pH > 12), and meanwhile the divalent or trivalent cations will precipitate in such a high pH solution, acetonitrile is used instead of water. Typically, LAC_{60} or DAC_{60} was dissolved in acetonitrile, and then the solutions were filtered through a PTFE syringe filter with a 200 nm pore size. The filtered solutions were loaded into a 20 mL vial, and additional $ZnCl_2$/small chiral molecule solutions (MeCN, prefiltered) were added accordingly.

■ ASSOCIATED CONTENT

Supporting Information

The Supporting Information is available free of charge at https://pubs.acs.org/doi/10.1021/acs.langmuir.0c00611.

Sample preparations, detailed synthetic procedures and characterizations of chiral AC_{60} macroions, counterions, and co-ions, ITC fitting curves, AFM analysis, and other SLS/DLS results (PDF)

■ AUTHOR INFORMATION

Corresponding Author

Tianbo Liu − *Department of Polymer Science, The University of Akron, Akron, Ohio 44325, United States;* orcid.org/0000-0002-8181-1790; Email: tliu@uakron.edu

Authors

Jiancheng Luo − *Department of Polymer Science, The University of Akron, Akron, Ohio 44325, United States;* orcid.org/0000-0002-3766-4922

Songtao Ye − *Department of Polymer Science, The University of Akron, Akron, Ohio 44325, United States*

Putu Ustriyana − *Department of Polymer Science, The University of Akron, Akron, Ohio 44325, United States;* orcid.org/0000-0001-9804-3081

Benqian Wei − *Department of Polymer Science, The University of Akron, Akron, Ohio 44325, United States*

Jiahui Chen − *Department of Polymer Science, The University of Akron, Akron, Ohio 44325, United States;* orcid.org/0000-0002-3861-146X

Ehsan Raee − *Department of Polymer Science, The University of Akron, Akron, Ohio 44325, United States*

Yinghe Hu − *Department of Polymer Science, The University of Akron, Akron, Ohio 44325, United States*

Yuqing Yang − *Department of Polymer Science, The University of Akron, Akron, Ohio 44325, United States;* orcid.org/0000-0002-5407-5740

Yifan Zhou − *Department of Polymer Science, The University of Akron, Akron, Ohio 44325, United States*

Chrys Wesdemiotis − *Department of Polymer Science and Department of Chemistry, The University of Akron, Akron, Ohio 44325, United States*

Nita Sahai − *Department of Polymer Science, The University of Akron, Akron, Ohio 44325, United States;* orcid.org/0000-0003-3852-0557

Complete contact information is available at: https://pubs.acs.org/10.1021/acs.langmuir.0c00611

Notes

The authors declare no competing financial interest.

■ ACKNOWLEDGMENTS

T.L. acknowledges support by NSF (CHE1607138 and CHE1904397) and the University of Akron.

■ REFERENCES

(1) Berthod, A. Chiral Recognition Mechanisms. *Anal. Chem.* **2006**, *78*, 2093−2099.

(2) Gal, J. Louis Pasteur, Language, and Molecular Chirality. I. Background and Dissymmetry. *Chirality* **2011**, *23*, 1−16.

(3) Barron, L. D. Symmetry and Molecular Chirality. *Chem. Soc. Rev.* **1986**, *15*, 189−223.

(4) Kondepudi, D. K.; Kaufman, R. J.; Singh, N. Chiral Symmetry Breaking in Sodium Chlorate Crystallizaton. *Science* **1990**, *250*, 975.

(5) Addadi, L.; Weiner, S. Crystals, Asymmetry and Life. *Nature* **2001**, *411*, 753−755.

(6) Viedma, C. Chiral Symmetry Breaking During Crystallization: Complete Chiral Purity Induced by Nonlinear Autocatalysis and Recycling. *Phys. Rev. Lett.* **2005**, *94*, No. 065504.

(7) Ramirez, J.; He, F.; Lebrilla, C. B. Gas-Phase Chiral Differentiation of Amino Acid Guests in Cyclodextrin Hosts. *J. Am. Chem. Soc.* **1998**, *120*, 7387−7388.

(8) Cooks, R. G.; Zhang, D.; Koch, K. J.; Gozzo, F. C.; Eberlin, M. N. Chiroselective Self-Directed Octamerization of Serine: Implications for Homochirogenesis. *Anal. Chem.* **2001**, *73*, 3646−3655.

(9) Koch, K. J.; Gozzo, F. C.; Nanita, S. C.; Takats, Z.; Eberlin, M. N.; Cooks, R. G. Chiral Transmission between Amino Acids: Chirally Selective Amino Acid Substitution in the Serine Octamer as a Possible Step in Homochirogenesis. *Angew. Chem., Int. Ed.* **2002**, *41*, 1721−1724.

(10) Ariga, K.; Michinobu, T.; Nakanishi, T.; Hill, J. P. Chiral Recognition at the Air−Water Interface. *Curr. Opin. Colloid Interface Sci.* **2008**, *13*, 23−30.

(11) Elemans, J. A. A. W.; De Cat, I.; Xu, H.; De Feyter, S. Two-Dimensional Chirality at Liquid−Solid Interfaces. *Chem. Soc. Rev.* **2009**, *38*, 722−736.

(12) Feringa, B. L.; van Delden, R. A. Absolute Asymmetric Synthesis: The Origin, Control, and Amplification of Chirality. *Angew. Chem., Int. Ed.* **1999**, *38*, 3418−3438.

(13) Maruoka, K.; Ooi, T. Enantioselective Amino Acid Synthesis by Chiral Phase-Transfer Catalysis. *Chem. Rev.* **2003**, *103*, 3013−3028.

(14) Yoon, T. P.; Jacobsen, E. N. Privileged Chiral Catalysts. *Science* **2003**, *299*, 1691.

(15) Maroto, E. E.; Mateos, J.; Garcia-Borràs, M.; Osuna, S.; Filippone, S.; Herranz, M. Á.; Murata, Y.; Solà, M.; Martín, N. Enantiospecific cis−trans Isomerization in Chiral Fulleropyrrolidines: Hydrogen-Bonding Assistance in the Carbanion Stabilization in H2O@C60. *J. Am. Chem. Soc.* **2015**, *137*, 1190−1197.

(16) ten Cate, A. T.; Dankers, P. Y. W.; Kooijman, H.; Spek, A. L.; Sijbesma, R. P.; Meijer, E. W. Enantioselective Cyclization of Racemic Supramolecular Polymers. *J. Am. Chem. Soc.* **2003**, *125*, 6860−6861.
(17) Mateos-Timoneda, M. A.; Crego-Calama, M.; Reinhoudt, D. N. Supramolecular Chirality of Self-Assembled Systems in Solution. *Chem. Soc. Rev.* **2004**, *33*, 363−372.
(18) Jin, W.; Fukushima, T.; Niki, M.; Kosaka, A.; Ishii, N.; Aida, T. Self-Assembled Graphitic Nanotubes with One-Handed Helical Arrays of A Chiral Amphiphilic Molecular Graphene. *Proc. Natl. Acad. Sci. U.S.A.* **2005**, *102*, 10801.
(19) Liu, M.; Zhang, L.; Wang, T. Supramolecular Chirality in Self-Assembled Systems. *Chem. Rev.* **2015**, *115*, 7304−7397.
(20) Roche, C.; Sun, H.-J.; Leowanawat, P.; Araoka, F.; Partridge, B. E.; Peterca, M.; Wilson, D. A.; Prendergast, M. E.; Heiney, P. A.; Graf, R.; Spiess, H. W.; Zeng, X.; Ungar, G.; Percec, V. A Supramolecular Helix that Disregards Chirality. *Nat. Chem.* **2016**, *8*, 80−89.
(21) Beaudoin, D.; Rominger, F.; Mastalerz, M. Chiral Self-Sorting of [2+3] Salicylimine Cage Compounds. *Angew. Chem., Int. Ed.* **2017**, *56*, 1244−1248.
(22) Ma, W.; Xu, L.; de Moura, A. F.; Wu, X.; Kuang, H.; Xu, C.; Kotov, N. A. Chiral Inorganic Nanostructures. *Chem. Rev.* **2017**, *117*, 8041−8093.
(23) Perry, S. L.; Leon, L.; Hoffmann, K. Q.; Kade, M. J.; Priftis, D.; Black, K. A.; Wong, D.; Klein, R. A.; Pierce, C. F.; Margossian, K. O.; Whitmer, J. K.; Qin, J.; de Pablo, J. J.; Tirrell, M. Chirality-Selected Phase Behaviour in Ionic Polypeptide Complexes. *Nat. Commun.* **2015**, *6*, No. 6052.
(24) Oda, R.; Artzner, F.; Laguerre, M.; Huc, I. Molecular Structure of Self-Assembled Chiral Nanoribbons and Nanotubules Revealed in the Hydrated State. *J. Am. Chem. Soc.* **2008**, *130*, 14705−14712.
(25) Bonner, W. A. The Origin and Amplification of Biomolecular Chirality. *Origins Life Evol. Biospheres* **1991**, *21*, 59−111.
(26) Blackmond, D. G. The Origin of Biological Homochirality. *Cold Spring Harbor Perspect. Biol.* **2010**, *2*, No. a002147.
(27) Breslow, R. A Likely Possible Origin of Homochirality in Amino Acids and Sugars on Prebiotic Earth. *Tetrahedron Lett.* **2011**, *52*, 2028−2032.
(28) Guijarro, A.; Yus, M. *The Origin of Chirality in the Molecules of Life: A Revision from Awareness to the Current Theories and Perspectives of This Unsolved Problem*; Royal Society of Chemistry, 2008.
(29) Ziserman, L.; Lee, H.-Y.; Raghavan, S. R.; Mor, A.; Danino, D. Unraveling the Mechanism of Nanotube Formation by Chiral Self-Assembly of Amphiphiles. *J. Am. Chem. Soc.* **2011**, *133*, 2511−2517.
(30) Kang, J.; Miyajima, D.; Itoh, Y.; Mori, T.; Tanaka, H.; Yamauchi, M.; Inoue, Y.; Harada, S.; Aida, T. C5-Symmetric Chiral Corannulenes: Desymmetrization of Bowl Inversion Equilibrium via "Intramolecular" Hydrogen-Bonding Network. *J. Am. Chem. Soc.* **2014**, *136*, 10640−10644.
(31) Anetai, H.; Takeda, T.; Hoshino, N.; Araki, Y.; Wada, T.; Yamamoto, S.; Mitsuishi, M.; Tsuchida, H.; Ogoshi, T.; Akutagawa, T. Circular Polarized Luminescence of Hydrogen-Bonded Molecular Assemblies of Chiral Pyrene Derivatives. *J. Phys. Chem. C* **2018**, *122*, 6323−6331.
(32) Tam, A. Y.-Y.; Wong, K. M.-C.; Yam, V. W.-W. Influence of Counteranion on the Chiral Supramolecular Assembly of Alkynylplatinum(II) Terpyridyl Metallogels That Are Stabilised by Pt···Pt and $\pi-\pi$ Interactions. *Chem. Eur. J.* **2009**, *15*, 4775−4778.
(33) Danila, I.; Riobé, F.; Piron, F.; Puigmartí-Luis, J.; Wallis, J. D.; Linares, M.; Ågren, H.; Beljonne, D.; Amabilino, D. B.; Avarvari, N. Hierarchical Chiral Expression from the Nano- to Mesoscale in Synthetic Supramolecular Helical Fibers of a Nonamphiphilic C3-Symmetrical π-Functional Molecule. *J. Am. Chem. Soc.* **2011**, *133*, 8344−8353.
(34) Rekharsky, M.; Inoue, Y. Chiral Recognition Thermodynamics of β-Cyclodextrin: The Thermodynamic Origin of Enantioselectivity and the Enthalpy−Entropy Compensation Effect. *J. Am. Chem. Soc.* **2000**, *122*, 4418−4435.
(35) Miyauchi, M.; Takashima, Y.; Yamaguchi, H.; Harada, A. Chiral Supramolecular Polymers Formed by Host−Guest Interactions. *J. Am. Chem. Soc.* **2005**, *127*, 2984−2989.
(36) Yin, P.; Zhang, Z.-M.; Lv, H.; Li, T.; Haso, F.; Hu, L.; Zhang, B.; Bacsa, J.; Wei, Y.; Gao, Y.; Hou, Y.; Li, Y.-G.; Hill, C. L.; Wang, E.-B.; Liu, T. Chiral Recognition and Selection during the Self-Assembly Process of Protein-Mimic Macroanions. *Nat. Commun.* **2015**, *6*, No. 6475.
(37) Narayanan, J.; Liu, X. Y. Protein Interactions in Undersaturated and Supersaturated Solutions: A Study Using Light and X-Ray Scattering. *Biophys. J.* **2003**, *84*, 523−532.
(38) Tavares, F. W.; Bratko, D.; Blanch, H. W.; Prausnitz, J. M. Ion-Specific Effects in the Colloid−Colloid or Protein−Protein Potential of Mean Force: Role of Salt−Macroion van der Waals Interactions. *J. Phys. Chem. B* **2004**, *108*, 9228−9235.
(39) Lund, M.; Jönsson, B. On the Charge Regulation of Proteins. *Biochemistry* **2005**, *44*, 5722−5727.
(40) Liu, T. Hydrophilic Macroionic Solutions: What Happens When Soluble Ions Reach the Size of Nanometer Scale? *Langmuir* **2010**, *26*, 9202−9213.
(41) Buchecker, T.; Schmid, P.; Renaudineau, S.; Diat, O.; Proust, A.; Pfitzner, A.; Bauduin, P. Polyoxometalates in the Hofmeister series. *Chem. Commun.* **2018**, *54*, 1833−1836.
(42) Misra, A.; Kozma, K.; Streb, C.; Nyman, M. Beyond Charge Balance: Counter-Cations in Polyoxometalate Chemistry. *Angew. Chem., Int. Ed.* **2020**, *59*, 596−612.
(43) Ansari, A.; Jones, C. M.; Henry, E. R.; Hofrichter, J.; Eaton, W. A. The Role of Solvent Viscosity in the Dynamics of Protein Conformational Changes. *Science* **1992**, *256*, 1796.
(44) Shang, L.; Wang, Y.; Jiang, J.; Dong, S. pH-Dependent Protein Conformational Changes in Albumin:Gold Nanoparticle Bioconjugates: A Spectroscopic Study. *Langmuir* **2007**, *23*, 2714−2721.
(45) Liu, T.; Diemann, E.; Li, H.; Dress, A. W. M.; Müller, A. Self-Assembly in Aqueous Solution of Wheel-Shaped Mo154 Oxide Clusters into Vesicles. *Nature* **2003**, *426*, 59−62.
(46) Li, H.; Luo, J.; Liu, T. Modification of the Solution Behavior of Pd12L24 Metal−Organic Nanocages via PEGylation. *Chem. Eur. J.* **2016**, *22*, 17949−17952.
(47) Yin, P.; Lin, Z.; Wu, J.; Hsu, C.-H.; Chen, X.; Zhou, J.; Lu, P.; Eghtesadi, S. A.; Yu, X.; Cheng, S. Z. D.; Liu, T. Charge-Regulated Spontaneous, Reversible Self-Assembly of the Carboxylic Acid-Functionalized Hydrophilic Fullerene Macroanions in Dilute Solution. *Macromolecules* **2015**, *48*, 725−731.
(48) Zhang, J.; Li, D.; Liu, G.; Glover, K. J.; Liu, T. Lag Periods During the Self-Assembly of {Mo72Fe30} Macroions: Connection to the Virus Capsid Formation Process. *J. Am. Chem. Soc.* **2009**, *131*, 15152−15159.
(49) Pigga, J. M.; Teprovich, J. A.; Flowers, R. A.; Antonio, M. R.; Liu, T. Selective Monovalent Cation Association and Exchange around Keplerate Polyoxometalate Macroanions in Dilute Aqueous Solutions. *Langmuir* **2010**, *26*, 9449−9456.
(50) Haso, F.; Luo, J.; Bassil, B. S.; Artetxe, B.; Zhou, J.; Yin, P.; Reinoso, S.; Gutiérrez-Zorrilla, J. M.; Kortz, U.; Liu, T. Effect of Directional Hydrogen Bonding on the Self-Assembly of Anisotropically-Shaped Macroions. *ChemistrySelect* **2016**, *1*, 4345−4349.
(51) Luo, J.; Chen, K.; Yin, P.; Li, T.; Wan, G.; Zhang, J.; Ye, S.; Bi, X.; Pang, Y.; Wei, Y.; Liu, T. Effect of Cation−π Interaction on Macroionic Self-Assembly. *Angew. Chem., Int. Ed.* **2018**, *57*, 4067−4072.
(52) Kroto, H. W.; Heath, J. R.; O'Brien, S. C.; Curl, R. F.; Smalley, R. E. C60: Buckminsterfullerene. *Nature* **1985**, *318*, 162−163.
(53) Dresselhaus, M. S.; Dresselhaus, G.; Eklund, P. C. *Science of Fullerenes and Carbon Nanotubes: Their Properties and Applications*; Elsevier, 1996.
(54) Hirsch, A.; Brettreich, M. *Fullerenes: Chemistry and Reactions*; John Wiley & Sons, 2006.
(55) Nakamura, E.; Isobe, H. Functionalized Fullerenes in Water. The First 10 Years of Their Chemistry, Biology, and Nanoscience. *Acc. Chem. Res.* **2003**, *36*, 807−815.

https://dx.doi.org/10.1021/acs.langmuir.0c00611
Langmuir 2020, 36, 4702−4710

(56) Bingel, C. Cyclopropanierung von Fullerenen. *Chem. Ber.* **1993**, *126*, 1957−1959.
(57) Hirsch, A.; Lamparth, I.; Groesser, T.; Karfunkel, H. R. Regiochemistry of Multiple Additions to the Fullerene Core: Synthesis of a Th-Symmetric Hexakis Adduct of C60 with Bis(ethoxycarbonyl)methylene. *J. Am. Chem. Soc.* **1994**, *116*, 9385−9386.
(58) Hirsch, A.; Vostrowsky, O. C60 Hexakisadducts with an Octahedral Addition Pattern − A New Structure Motif in Organic Chemistry. *Eur. J. Org. Chem.* **2001**, *2001*, 829−848.
(59) Sánchez-Navarro, M.; Muñoz, A.; Illescas, B. M.; Rojo, J.; Martín, N. [60]Fullerene as Multivalent Scaffold: Efficient Molecular Recognition of Globular Glycofullerenes by Concanavalin A. *Chem. Eur. J.* **2011**, *17*, 766−769.
(60) Liu, G.; Liu, T. Strong Attraction among the Fully Hydrophilic {Mo72Fe30} Macroanions. *J. Am. Chem. Soc.* **2005**, *127*, 6942−6943.
(61) Provencher, S. W. CONTIN: A General Purpose Constrained Regularization Program for Inverting Noisy Linear Algebraic and Integral Equations. *Comput. Phys. Commun.* **1982**, *27*, 229−242.
(62) Hiemenz, P. C. *Principles of Colloid and Surface Chemistry*; M. Dekker: New York, 1986; Vol *188*.
(63) Freire, E.; Mayorga, O. L.; Straume, M. Isothermal Titration Calorimetry. *Anal. Chem.* **1990**, *62*, 950A−959A.
(64) Leavitt, S.; Freire, E. Direct Measurement of Protein Binding Energetics by Isothermal Titration Calorimetry. *Curr. Opin. Struct. Biol.* **2001**, *11*, 560−566.
(65) VanPelt, C. E.; Crooks, W. J.; Choppin, G. R. Thermodynamic Constant Determination for the Complexation of Trivalent Lanthanides with Polyoxometalates. *Inorg. Chim. Acta* **2002**, *340*, 1−7.
(66) Marcus, Y.; Hefter, G. Ion Pairing. *Chem. Rev.* **2006**, *106*, 4585−4621.
(67) Luo, J.; Ye, S.; Li, T.; Sarnello, E.; Li, H.; Liu, T. Distinctive Trend of Metal Binding Affinity via Hydration Shell Breakage in Nanoconfined Cavity. *J. Phys. Chem. C* **2019**, *123*, 14825−14833.
(68) Barry, E.; Hensel, Z.; Dogic, Z.; Shribak, M.; Oldenbourg, R. Entropy-Driven Formation of a Chiral Liquid-Crystalline Phase of Helical Filaments. *Phys. Rev. Lett.* **2006**, *96*, No. 018305.
(69) Sisco, S. W.; Moore, J. S. Homochiral Self-Sorting of BINOL Macrocycles. *Chem. Sci.* **2014**, *5*, 81−85.
(70) Atcher, J.; Bujons, J.; Alfonso, I. Entropy-Driven Homochiral Self-Sorting of A Dynamic Library. *Chem. Commun.* **2017**, *53*, 4274−4277.
(71) Park, S.-J.; Seo, M.-K. Chapter 1 - Intermolecular Force. In *Interface Science and Technology*; Park, S.-J.; Seo, M.-K., Eds.; Elsevier, 2011; Vol *18*, pp 1−57.
(72) Schmitz, K. S. Macroion Clustering in Solutions and Suspensions: The Roles of Microions and Solvent. *J. Phys. Chem. B* **2009**, *113*, 2624−2638.
(73) Li, Y.; Girard, M.; Shen, M.; Millan, J. A.; Olvera de la Cruz, M. Strong attractions and repulsions mediated by monovalent salts. *Proc. Natl. Acad. Sci. U.S.A.* **2017**, *114*, 11838.
(74) Lima, E. R. A.; Boström, M.; Horinek, D.; Biscaia, E. C.; Kunz, W.; Tavares, F. W. Co-Ion and Ion Competition Effects: Ion Distributions Close to a Hydrophobic Solid Surface in Mixed Electrolyte Solutions. *Langmuir* **2008**, *24*, 3944−3948.
(75) Zhang, Y.; Cremer, P. S. The Inverse and Direct Hofmeister Series for Lysozyme. *Proc. Natl. Acad. Sci. U.S.A.* **2009**, *106*, 15249.
(76) Salis, A.; Ninham, B. W. Models and Mechanisms of Hofmeister Effects in Electrolyte Solutions, and Colloid and Protein Systems Revisited. *Chem. Soc. Rev.* **2014**, *43*, 7358−7377.
(77) Okur, H. I.; Hladílková, J.; Rembert, K. B.; Cho, Y.; Heyda, J.; Dzubiella, J.; Cremer, P. S.; Jungwirth, P. Beyond the Hofmeister Series: Ion-Specific Effects on Proteins and Their Biological Functions. *J. Phys. Chem. B* **2017**, *121*, 1997−2014.
(78) Qi, B.; Guo, X.; Gao, Y.; Li, D.; Luo, J.; Li, H.; Eghtesadi, S. A.; He, C.; Duan, C.; Liu, T. Strong Co-Ion Effect via Cation−π Interaction on the Self-Assembly of Metal−Organic Cationic Macrocycles. *J. Am. Chem. Soc.* **2017**, *139*, 12020−12026.
(79) Salerno, K. M.; Frischknecht, A. L.; Stevens, M. J. Charged Nanoparticle Attraction in Multivalent Salt Solution: A Classical-Fluids Density Functional Theory and Molecular Dynamics Study. *J. Phys. Chem. B* **2016**, *120*, 5927−5937.
(80) Attard, P. Recent Advances in the Electric Double Layer in Colloid Science. *Curr. Opin. Colloid Interface Sci.* **2001**, *6*, 366−371.
(81) Ni, R.; Cao, D.; Wang, W. A Monte Carlo Study of Spherical Electrical Double Layer of Macroions−Polyelectrolytes Systems in Salt Free Solutions. *J. Phys. Chem. B* **2006**, *110*, 26232−26239.

https://dx.doi.org/10.1021/acs.langmuir.0c00611
Langmuir 2020, 36, 4702−4710